Origin of Vector Parasites in Numerical Maxwell Solutions

Daniel R. Lynch and Keith D. Paulsen, *Member, IEEE*

Abstract—**Dispersion relations are derived for conventional finite element and finite difference approximations of four versions of the Maxwell equations in the plane: the double-curl equation; the vector Helmholtz equation; the penalty equation; and the primitive, coupled Maxwell curl equations. Comparison with their analytic counterparts reveals the presence and origin of vector parasites. In each case there are no essential qualitative differences between the finite difference and finite element approaches per se; all of the issues surround the form of the differential equation underlying the discretization.**

For the double-curl and penalty methods, the dispersion relations are double-valued, admitting an extra, spurious dispersion surface of real-valued wavenumbers. As a result, low wavenumbers support both well-resolved and poorly resolved vector parasites. Additionally the "physical" modes in these solutions have nonzero divergence, such that satisfaction of divergence-free boundary conditions necessarily invokes the parasitic modes. The Helmholtz schemes have monotonic, single valued dispersion relations for divergence-free physical modes. Specification of divergence-free boundary conditions is sufficient to guarantee the absence of parasites. The primitive schemes have single-valued but folded (nonmonotonic) dispersion relations, supporting poorly resolved vector parasites at low wavenumbers. Use of a staggered finite difference grid eliminates these parasites and results in a dispersion relation identical to that for the Helmholtz scheme. In all cases where vector parasites arise the same essential weakness in the discretized form of either the first or cross-derivative is responsible. Overall, this analysis illuminates fatal weaknesses in the double-curl schemes considered, the reliance on a staggered mesh in the primitive schemes, and the strength of the vector Helmholtz schemes.

I. Introduction

THE occurrence of vector parasites in numerical solutions to Maxwell's equations has been reported by several investigators [1]–[7], especially in the finite element context. There are many options for dealing with these spurious solutions, including the use of special or staggered meshes [8]–[11], constrained bases and/or weighting functions [12]–[15], modified weak-form functionals [4], [7], [16], and the use of potentials rather than the physical fields as primary variables [17]. Despite the chronic nature of this problem, a coherent explanation with predictive power, i.e., one that provides criteria for *a priori* selection among the various numerical options, has remained elusive.

In this paper we show the origin of 2-D vector parasites in the dispersion relations which we derive for basic finite difference (FD) and finite element (FE) discretizations of four versions of the Maxwell equations:

- the double-curl equation (FDD and FED schemes)
- the vector Helmholtz equation (FDH and FEH schemes)
- the penalty method (FDP and FEP schemes)
- the primitive (single-curl) Maxwell equations (FDM and FEM schemes)

All are implemented on uniform square grids and use equivalent-order approximations—second-order centered differences for the FD methods, and Galerkin approximations with C^0 bilinear scalar bases for the FE methods.

There are three essential findings. First, a *double-valued dispersion relation* characterizes both FE and FD discretization of the double-curl equation and its related "penalty" form. This generates two dispersion surfaces, one "physical" and the other spurious. As a result, two families of solutions are supported by a given wavenumber, one of which is completely unphysical. The FD and FE versions of these equations are not materially different in this fundamental behavior. Both FD and FE methods based on the Helmholtz equation possess well-behaved, monotonic dispersion relations which resemble the exact analytic version. This single relation characterizes both physical and spurious modes alike, and can be viewed as the congruence of the two families in the penalty method when $p = 1$.

The second essential finding relates to the manner in which physical and spurious modes are combined in driven problems. For the discretized double-curl and penalty methods the two modes are not perfectly sorted—specifically, the physical modes have nonzero divergence, and the spurious modes have nonzero curl. As a result, a physically well posed boundary condition with zero divergence will *necessarily* invoke a blend of both modes. By contrast, the physical modes supported by the discretized Helmholtz schemes are *precisely* divergence-free. Therefore the potential for spurious modes is eliminated by the enforcement of physical boundary conditions. Among the FE methods examined here, only the Helmholtz scheme provides a physical solution to a physically forced problem, uncontaminated by vector parasites.

The fundamental flaw in the double-curl and penalty methods can be further traced to the numerical weakness of the cross-derivative term $\partial^2/\partial x\,\partial y$. This term converges more slowly at high resolution than its companions $\partial^2/\partial x^2$, etc.; at low resolution it is "folded," introducing an essential confusion between modes with short (e.g. $2\Delta x$) and long (e.g. ∞) wavelengths. These two weaknesses generate in turn the two types of parasites reported by Davies *et al.* [3] and in our own work [7]: well-resolved parasites with nonzero divergence and poorly resolved parasites at or near the mesh

Manuscript received February 16, 1990; revised October 10, 1990. This work was supported by the U.S. National Science Foundation under Grant CEE-8352226 and by the National Institutes of Health under Grants NIH/NCI CA45357 and CA37245.

The authors are with the Thayer School of Engineering, Dartmouth College, Hanover, NH 03755.

IEEE Log Number 9042352.

0018-9480/91/0300-0383$01.00 ©1991 IEEE

cutoff point in one of the spatial directions. We refer to these as type A and type B parasites, respectively.

The third essential finding is a *folded dispersion relation*, which characterizes the primitive schemes, supporting low-wavenumber parasites at coarse resolution. We refer to these as type C here. As above, the FD and FE expressions are not substantially different. However in the FD case the parasites are quickly and effectively eliminated by use of a staggered mesh. This strategy has proven successful in time-domain FD calculations; it remains somewhat unnatural in the FE context, where no unique, direct analog has emerged. The root cause of the folded dispersion relationship is the numerical first derivative in these schemes. It has the same fundamental confusion among long and short waves as does the cross-derivative described above.

The analysis here is of course limited to the numerical schemes and ideal, homogeneous grids selected. Within these limitations, however, it explains the occurrence of two types of vector parasites which have been reported in double-curl solutions; their reported absence in Helmholtz solutions; and the disappointing track record of the finite element method based on the primitive equations with conventional elements. As a tool, the dispersion analysis has explanatory and predictive power and is recommended as an analytical filter for other proposed methods for eliminating vector parasites. While no analysis is sufficient to guarantee freedom from *all* numerical pitfalls (e.g. those provoked by inappropriate or unphysical boundary conditions, material interfaces, etc.), if a given discretization fails this analysis it can be considered fundamentally flawed at the outset.

II. Analytic Solution

To begin, we review the dispersion relations for analytic solutions in the plane. Throughout we assume solutions of the form

$$\boldsymbol{E}(x,y)=\begin{Bmatrix}E_x(x,y)\\E_y(x,y)\end{Bmatrix}=\begin{Bmatrix}E_{x0}\\E_{y0}\end{Bmatrix}e^{i(\sigma x+\gamma y)} \tag{1}$$

where (E_{x0},E_{y0}) are unknown constants. Differentiating (1) allows us to define the magnitudes of the divergence and curl, D and C:

$$\nabla\cdot\boldsymbol{E}=De^{i(\sigma x+\gamma y)} \tag{2}$$

$$\nabla\times\boldsymbol{E}=Ce^{i(\sigma x+\gamma y)}\hat{z} \tag{3}$$

where

$$D\equiv i(\sigma E_{x0}+\gamma E_{y0}) \tag{4}$$

$$C\equiv i(\sigma E_{y0}-\gamma E_{x0}) \tag{5}$$

Equations (4) and (5) may be inverted:

$$E_{x0}=-i(\sigma D-\gamma C)/(\sigma^2+\gamma^2) \tag{6}$$

$$E_{y0}=-i(\sigma C+\gamma D)/(\sigma^2+\gamma^2) \tag{7}$$

and we recall that the pairs (D,C) and (E_{x0},E_{y0}) are equivalent; i.e., either pair is sufficient to describe a wave with a given wavenumber pair (σ,γ).

We first consider the double-curl equation

$$\nabla\times\nabla\times\boldsymbol{E}-k^2\boldsymbol{E}=0 \tag{8}$$

which may be reexpressed in matrix form:

$$\begin{bmatrix}-\dfrac{\partial^2}{\partial y^2}-k^2 & \dfrac{\partial^2}{\partial y\partial x}\\ \dfrac{\partial^2}{\partial x\partial y} & -\dfrac{\partial^2}{\partial x^2}-k^2\end{bmatrix}\begin{Bmatrix}E_x\\E_y\end{Bmatrix}=\begin{Bmatrix}0\\0\end{Bmatrix}. \tag{9}$$

Substitution of (1) yields

$$\begin{bmatrix}\gamma^2-k^2 & -\gamma\sigma\\ -\sigma\gamma & \sigma^2-k^2\end{bmatrix}\begin{Bmatrix}E_{x0}\\E_{y0}\end{Bmatrix}=\begin{Bmatrix}0\\0\end{Bmatrix}. \tag{10}$$

For nontrivial solutions the matrix in (10) must be singular:

$$(\gamma^2-k^2)(\sigma^2-k^2)-\sigma^2\gamma^2=0 \tag{11}$$

or equivalently

$$k^2(k^2-\sigma^2-\gamma^2)=0. \tag{12}$$

In (12) there are two obvious sets of solutions: $S1$, in which $k^2=0$; and $S2$, in which $k^2=\sigma^2+\gamma^2$. $S1$ is readily classified as curl-free by substituting $k^2=0$ into the matrix equation (10) and solving for the required relationship between E_{x0} and E_{y0}. The divergence may be found in turn from (4). Similarly for $S2$, we find $D=0$ and obtain the curl from (5). Summarizing, the double-curl equation admits two sets of solutions:

$$S1\text{: } k^2=0;\quad C=0;\quad D=i\frac{E_{x0}}{\sigma}(\sigma^2+\gamma^2)=i\frac{E_{y0}}{\gamma}(\sigma^2+\gamma^2) \tag{13}$$

$$S2\text{: } k^2=\sigma^2+\gamma^2;\quad D=0;\quad C=-i\frac{E_{x0}}{\gamma}(\sigma^2+\gamma^2)=i\frac{E_{y0}}{\sigma}(\sigma^2+\gamma^2). \tag{14}$$

Next consider the Helmholtz equation

$$\nabla^2\boldsymbol{E}+k^2\boldsymbol{E}=0 \tag{15}$$

which in matrix form is

$$\begin{bmatrix}\dfrac{\partial^2}{\partial x^2}+\dfrac{\partial^2}{\partial y^2}+k^2 & 0\\ 0 & \dfrac{\partial^2}{\partial x^2}+\dfrac{\partial^2}{\partial y^2}+k^2\end{bmatrix}\begin{Bmatrix}E_x\\E_y\end{Bmatrix}=\begin{Bmatrix}0\\0\end{Bmatrix}. \tag{16}$$

Substitution of (1) yields

$$\begin{bmatrix}-\sigma^2-\gamma^2+k^2 & 0\\ 0 & -\sigma^2-\gamma^2+k^2\end{bmatrix}\begin{Bmatrix}E_{x0}\\E_{y0}\end{Bmatrix}=\begin{Bmatrix}0\\0\end{Bmatrix} \tag{17}$$

for which nontrivial solutions exist only when $k^2=\sigma^2+\gamma^2$, i.e., the identical dispersion relation as for set $S2$ above. In this case however, E_{x0} and E_{y0} are completely uncoupled in (16). Therefore, (17) provides no information about (E_{x0},E_{y0}), and D and C are completely unconstrained. These solutions are therefore a superset of $S2$ above. Without loss of generality we divide them as follows:

$$S1'\text{: } k^2=\sigma^2+\gamma^2;\quad C=0;\quad D=i\frac{E_{x0}}{\sigma}(\sigma^2+\gamma^2) \tag{18a}$$

$$S2\text{: } k^2=\sigma^2+\gamma^2;\quad D=0;\quad C=-i\frac{E_{x0}}{\gamma}(\sigma^2+\gamma^2) \tag{18b}$$

with $S2$ exactly as in the double-curl equation, and $S1'$ a shifted version of $S1$.

Next we consider the penalty method, based on the composite equation

$$\nabla \times \nabla \times E - p\nabla(\nabla \cdot E) - k^2 E = 0 \tag{19}$$

where p is the dimensionless penalty factor. In matrix form we have

$$\begin{bmatrix} -\frac{\partial^2}{\partial y^2} - p\frac{\partial^2}{\partial x^2} - k^2 & (1-p)\frac{\partial^2}{\partial y\,\partial x} \\ (1-p)\frac{\partial^2}{\partial x\,\partial y} & -\frac{\partial^2}{\partial x^2} - p\frac{\partial^2}{\partial y^2} - k^2 \end{bmatrix} \begin{Bmatrix} E_x \\ E_y \end{Bmatrix} = \begin{Bmatrix} 0 \\ 0 \end{Bmatrix}. \tag{20}$$

Substitution of (1) gives

$$\begin{bmatrix} \gamma^2 + p\sigma^2 - k^2 & -(1-p)\gamma\sigma \\ -(1-p)\sigma\gamma & \sigma^2 + p\gamma^2 - k^2 \end{bmatrix} \begin{Bmatrix} E_{x0} \\ E_{y0} \end{Bmatrix} = \begin{Bmatrix} 0 \\ 0 \end{Bmatrix} \tag{21}$$

and the dispersion relation satisfies

$$(k^2 - p\sigma^2 - p\gamma^2)(k^2 - \sigma^2 - \gamma^2) = 0. \tag{22}$$

The two sets of solutions are

$$S1'': k^2 = p(\sigma^2 + \gamma^2); \quad C = 0; \quad D = i\frac{E_{x0}}{\sigma}(\sigma^2 + \gamma^2) \tag{23}$$

$$S2: k^2 = \sigma^2 + \gamma^2; \quad D = 0; \quad C = -i\frac{E_{x0}}{\gamma}(\sigma^2 + \gamma^2). \tag{24}$$

$S2$ is exactly the same as in the double-curl and Helmholtz equations; $S1''$ is a shifted version of $S1$.

Finally, we consider the coupled, single-curl Maxwell equations

$$\nabla \times H = -i\omega\epsilon E \tag{25}$$

$$\nabla \times E = i\omega\mu H. \tag{26}$$

We refer to these as primitive because they are the unaltered forms from which the double-curl and Helmholtz equations are derived by differentiation. In matrix form, we have

$$\begin{bmatrix} i\omega\epsilon & 0 & \frac{\partial}{\partial y} \\ 0 & i\omega\epsilon & -\frac{\partial}{\partial x} \\ \frac{\partial}{\partial y} & -\frac{\partial}{\partial x} & i\omega\mu \end{bmatrix} \begin{Bmatrix} E_x \\ E_y \\ H_z \end{Bmatrix} = \begin{Bmatrix} 0 \\ 0 \\ 0 \end{Bmatrix}. \tag{27}$$

Introduction of (1) and its equivalent for H_z gives

$$\begin{bmatrix} i\omega\epsilon & 0 & i\gamma \\ 0 & i\omega\epsilon & -i\sigma \\ i\gamma & -i\sigma & i\omega\mu \end{bmatrix} \begin{Bmatrix} E_{x0} \\ E_{y0} \\ H_{z0} \end{Bmatrix} = \begin{Bmatrix} 0 \\ 0 \\ 0 \end{Bmatrix} \tag{28}$$

and the singularity of (28) provides the dispersion relation

$$\omega\epsilon(k^2 - \sigma^2 - \gamma^2) = 0 \tag{29}$$

where $k^2 \equiv (\omega\mu)(\omega\epsilon)$. The primitive equations support exactly the sets $S1$ and $S2$ as in the double-curl equation. Substitution of (29) into (28) confirms that (D,C) are also identical to the double-curl case.

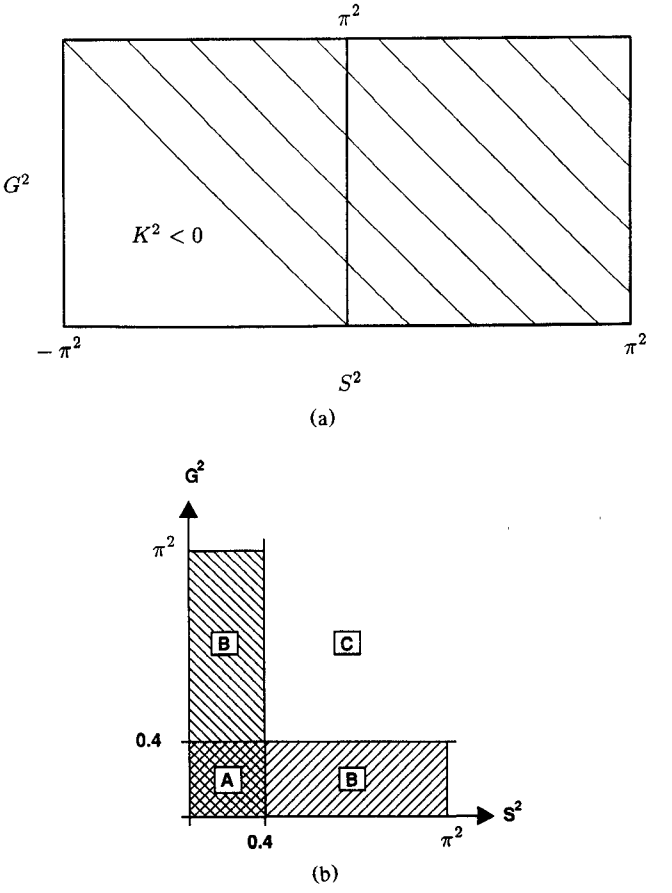

Fig. 1. (a) Contours of the dimensionless analytic dispersion relation for solution sets $S2$, displayed in (S^2, G^2) space. (b) Zones of potential parasites: Type A—well resolved in both directions; type B—well resolved in one direction, poorly resolved in the other; type C—poorly resolved in both directions.

All of these versions of the Maxwell equations share the physical solution set $S2$ with $D = 0$; and the various sets $S1, S1', S1''$ all have $C = 0$. For driven problems, the response is restricted to $S2$ in different ways. $S1$ is ruled out in double-curl and primitive solutions *a priori* for nonzero k^2. For the other operators, $S1'$ and $S1''$ are supported at nonzero k^2 and thus in general they may contaminate the solution, depending on the boundary conditions. *The property $D = 0$ of $S2$ is critical in these cases.* Specification of physical boundary conditions with $D = 0$ is sufficient to guarantee that the solution lies entirely in $S2$. As discussed below, numerical schemes which emulate $S1'$ or $S1''$ or which through discretization error produce shifted versions of $S1$ will *necessarily* be contaminated by spurious modes unless $D = 0$ for the corresponding set $S2$.

In Fig. 1(a) we display for reference the dispersion relation (14) for the physical set $S2$. We introduce a mesh spacing h and plot the dimensionless quantities $K^2 \equiv (kh)^2$ as a function of $S^2 \equiv (\sigma h)^2$ and $G^2 \equiv (\gamma h)^2$. We restrict attention to the Nyquist range $-\pi^2 < (S^2, G^2) < \pi^2$ and to quadrants I and II. Quadrant III supports only $k^2 < 0$; and quadrant IV is a mirror image of quadrant II. In Fig. 1(b) we delineate three zones A, B, and C, in which we will focus our search for parasites of type A (well resolved in both directions), type B (well resolved in one direction, poorly resolved in the other), and type C (poorly resolved in both directions). We

TABLE I
DIFFERENCE OPERATORS FOR FD AND FE APPROXIMATIONS

	FD	FE
$\left.\frac{\partial^2\phi}{\partial x^2}\right\|_{ij}$	$\frac{\phi_{i+1,j}-2\phi_{i,j}+\phi_{i-1,j}}{h^2}$	$\frac{1}{6}\left(\frac{\phi_{i+1,j+1}-2\phi_{i,j+1}+\phi_{i-1,j+1}}{h^2}\right)+\frac{4}{6}\left(\frac{\phi_{i+1,j}-2\phi_{i,j}+\phi_{i-1,j}}{h^2}\right)+\frac{1}{6}\left(\frac{\phi_{i+1,j-1}-2\phi_{i,j-1}+\phi_{i-1,j-1}}{h^2}\right)$
$\left.\frac{\partial^2\phi}{\partial y^2}\right\|_{ij}$	$\frac{\phi_{i,j+1}-2\phi_{i,j}+\phi_{i,j-1}}{h^2}$	$\frac{1}{6}\left(\frac{\phi_{i+1,j+1}-2\phi_{i+1,j}+\phi_{i+1,j-1}}{h^2}\right)+\frac{4}{6}\left(\frac{\phi_{i,j+1}-2\phi_{i,j}+\phi_{i,j-1}}{h^2}\right)+\frac{1}{6}\left(\frac{\phi_{i-1,j+1}-2\phi_{i-1,j}+\phi_{i-1,j-1}}{h^2}\right)$
$\left.\frac{\partial^2\phi}{\partial x\partial y}\right\|_{ij}$	$\frac{\phi_{i+1,j+1}-\phi_{i-1,j+1}-\phi_{i+1,j-1}+\phi_{i-1,j-1}}{4h^2}$	$\frac{\phi_{i+1,j+1}-\phi_{i-1,j+1}-\phi_{i+1,j-1}+\phi_{i-1,j-1}}{4h^2}$
$\left.\frac{\partial\phi}{\partial x}\right\|_{ij}$	$\frac{\phi_{i+1,j}-\phi_{i-1,j}}{2h}$	$\frac{1}{6}\left(\frac{\phi_{i+1,j+1}-\phi_{i-1,j+1}}{2h}\right)+\frac{4}{6}\left(\frac{\phi_{i+1,j}-\phi_{i-1,j}}{2h}\right)+\frac{1}{6}\left(\frac{\phi_{i+1,j-1}-\phi_{i-1,j-1}}{2h}\right)$
$\left.\frac{\partial\phi}{\partial y}\right\|_{ij}$	$\frac{\phi_{i,j+1}-\phi_{i,j-1}}{2h}$	$\frac{1}{6}\left(\frac{\phi_{i+1,j+1}-\phi_{i+1,j-1}}{2h}\right)+\frac{4}{6}\left(\frac{\phi_{i,j+1}-\phi_{i,j-1}}{2h}\right)+\frac{1}{6}\left(\frac{\phi_{i-1,j+1}-\phi_{i-1,j-1}}{2h}\right)$
$\phi\|_{ij}$	ϕ_{ij}	$\frac{1}{6}\left(\frac{\phi_{i+1,j+1}+4\phi_{i,j+1}+\phi_{i-1,j+1}}{6}\right)+\frac{4}{6}\left(\frac{\phi_{i+1,j}+4\phi_{i,j}+\phi_{i-1,j}}{6}\right)+\frac{1}{6}\left(\frac{\phi_{i+1,j-1}+4\phi_{i,j-1}+\phi_{i-1,j-1}}{6}\right)$

arbitrarily define *well resolved* as S^2 and/or $G^2 < 0.4$, i.e., roughly ten or more nodes per wavelength.

III. Difference Equations

Here we develop and record the difference equations for all of the discretized systems to be considered. We use the natural (i, j) node numbering system on a uniform mesh with constant mesh spacing $h \equiv \Delta x = \Delta y$. In the FD cases we use conventional second-order centered differences; all terms required for the double-curl, Helmholtz, and primitive equations appear in Table I, where we also show the individual Galerkin terms weighted with basis function (i, j). Each has been normalized by the factor h^2 to highlight the analogy with FD expressions.[1] On this simple square mesh, the FE expressions reproduce conventional FD forms, with spatial averaging by Simpson's rule in various ways. Note that both the FD and FE cross-derivative terms are identical.

Assuming a numerical solution of the form (1), the solutions at adjacent nodes in the x direction are shifted by the exponential factor

$$\phi_{i+1} = \phi_i e^{iS} \tag{30}$$

($S \equiv \sigma h$) and similarly for the y direction. Use of these shifts allows condensation of the difference expressions in Table I. For example, the second centered difference operator may be reduced to

$$\begin{aligned}\frac{1}{h^2}(\phi_{i+1}-2\phi_i+\phi_{i-1}) &= \frac{1}{h^2}(e^{iS}-2+e^{-iS})\phi_i \\ &= \frac{2}{h^2}(\cos(S)-1)\phi_i \\ &= -\sigma^2\left[\frac{\sin(S/2)}{S/2}\right]^2\phi_i.\end{aligned} \tag{31}$$

[1]Specifically, $\partial^2\phi/\partial x^2$ for the FE method is $1/h^2\langle(\partial^2\phi/\partial x^2)\psi_{ij}\rangle = -1/h^2\langle(\partial\phi/\partial x)(\partial\psi_{ij}/\partial x)\rangle$, with ψ_{ij} the basis function centered at node (i, j) and $\langle\ \rangle$ indicating integration over the plane. The other terms are similarly defined.

TABLE II
DEFINITION OF DISCRETIZATION FACTORS FOR SOLUTIONS OF THE FORM $\phi = \phi_{ij} e^{i(\sigma x + \gamma y)}$ ($\Delta x = \Delta y = h$ IS THE MESH SPACING; $S \equiv \sigma h$; $G \equiv \gamma h$)

$A_x = \dfrac{4+2\cos(S)}{6}$	$A_y = \dfrac{4+2\cos(G)}{6}$
$B_x = \dfrac{\sin(S)}{S}$	$B_y = \dfrac{\sin(G)}{G}$
$C_x = \dfrac{\sin(S/2)}{(S/2)}$	$C_y = \dfrac{\sin(G/2)}{(G/2)}$

TABLE III
DIFFERENCE OPERATORS AS IN TABLE I FOR $\phi = \phi_{ij} e^{i(\sigma x + \gamma y)}$

	FD	FE
$\left.\dfrac{\partial^2\phi}{\partial x^2}\right\|_{ij}$	$-C_x^2\sigma^2\phi_{ij}$	$-A_yC_x^2\sigma^2\phi_{ij}$
$\left.\dfrac{\partial^2\phi}{\partial y^2}\right\|_{ij}$	$-C_y^2\gamma^2\phi_{ij}$	$-A_xC_y^2\gamma^2\phi_{ij}$
$\left.\dfrac{\partial^2\phi}{\partial x\partial y}\right\|_{ij}$	$-B_xB_y\sigma\gamma\phi_{ij}$	$-B_xB_y\sigma\gamma\phi_{ij}$
$\left.\dfrac{\partial\phi}{\partial x}\right\|_{ij}$	$iB_x\sigma\phi_{ij}$	$iA_yB_x\sigma\phi_{ij}$
$\left.\dfrac{\partial\phi}{\partial y}\right\|_{ij}$	$iB_y\gamma\phi_{ij}$	$iA_xB_y\gamma\phi_{ij}$
$\phi\|_{ij}$	ϕ_{ij}	$A_xA_y\phi_{ij}$

The discretization factors A, B and C are defined in Table II and approach unity as the mesh is refined.

The effect of the finite difference approximation is concentrated in the discretization factor $C_x \equiv \sin(S/2)/(S/2)$. Similarly for the first centered difference we have

$$\frac{1}{2h}(\phi_{i+1} - \phi_{i-1}) = \frac{2i\sin(S)}{2h}\phi_i = i\sigma\left[\frac{\sin(S)}{S}\right]\phi_i \quad (32)$$

which defines a second discretization factor $B_x \equiv \sin(S)/S$. The Simpson rule operator defines a third factor, $A_x \equiv \dfrac{4+2\cos(S)}{6}$, since

$$\tfrac{1}{6}(\phi_{i+1} + 4\phi_i + \phi_{i-1}) = \left[\frac{4+2\cos(S)}{6}\right]\phi_i. \quad (33)$$

These discretization factors are summarized in Table II. They permit the compact expression in Table III of the various difference operators from Table I; in effect Table III is the Fourier transform of Table I. Note that all of the expressions in Table III approach their continuum counterparts as S and G become arbitrarily small.

In every case, only the averaging factors A_x, A_y distinguish the FE from the FD terms. We may therefore generalize all the mathematics by using the FE terms exclusively and retrieve the FD versions by setting A_x and A_y to unity when needed. Finally, note that both A_x and A_y are real and bounded by (1/3, 1). We may divide by either freely.

IV. DOUBLE-CURL SCHEMES

From Table III we assemble the relations for the discretized double-curl equations in the same form as (9) and (10):

$$\begin{bmatrix} A_xC_y^2\gamma^2 - A_xA_yk^2 & -B_yB_x\gamma\sigma \\ -B_xB_y\sigma\gamma & A_yC_x^2\sigma^2 - A_xA_yk^2 \end{bmatrix}\begin{Bmatrix} E_{xij} \\ E_{yij} \end{Bmatrix} = \begin{Bmatrix} 0 \\ 0 \end{Bmatrix}. \quad (34)$$

For nontrivial solutions the matrix must be singular, which leads to the discrete version of (12):

$$k^2\left(k^2 - \frac{C_x^2\sigma^2}{A_x} - \frac{C_y^2\gamma^2}{A_y}\right) + \sigma^2\gamma^2\left(\frac{C_x^2}{A_x}\frac{C_y^2}{A_y} - \frac{B_x^2}{A_x^2}\frac{B_y^2}{A_y^2}\right) = 0. \quad (35)$$

It is immediately clear that there is a problem with this scheme—there are two roots as in (12), but $k^2 = 0$ is not one of them:

$$k^2 = \frac{\kappa^2}{2} \pm \sqrt{\left(\frac{\kappa^2}{2}\right)^2 - \epsilon^2} \quad (36)$$

where

$$\kappa^2 \equiv \frac{C_x^2\sigma^2}{A_x} + \frac{C_y^2\gamma^2}{A_y} \quad (37)$$

and

$$\epsilon^2 \equiv \sigma^2\gamma^2\left(\frac{C_x^2}{A_x}\frac{C_y^2}{A_y} - \frac{B_x^2}{A_x^2}\frac{B_y^2}{A_y^2}\right). \quad (38)$$

Note that κ^2 is an intuitively appealing emulation of the analytic relation (14) and that $\epsilon^2 > 0$ in the first quadrant.

A. FDD Scheme

Examination of the FD version of (36) in the first quadrant is especially revealing. For small S and G, the two values of k^2 approach $(0, \kappa^2)$ asymptotically, imitating the analytic sets $S1$ and $S2$. However the negative option results in $k^2 > 0$ *for all finite* h. We therefore identify the negative option in (36) as the spurious value, and the positive option as the "physical" one. The culprit here is the fact that $B^2 < C^2$. Essentially the cross-derivative is obtained at half the resolution as the other second derivatives; therefore ϵ^2 never quite reduces to zero. This subtle imbalance allows well-resolved but spurious solutions approximating set $S1$ to exist at low $k^2 > 0$—the type A parasite. As the resolution gets coarser (higher S or G) the discrepancy between B and C grows, since σC_x increases with σ monotonically toward the Nyquist cutoff $S = \pi$, but σB_x peaks at $S = \pi/2$ and folds back to zero at the Nyquist point. Thus at large S and/or G, the FDD scheme is fundamentally confused, its cross-derivative unable to distinguish very long from very short wavelengths. For a fixed, well-resolved G, increasing values of S support larger spurious values of k^2—the type B parasite.

In Fig. 2 we plot both values of K^2 from (36) versus S^2, for G^2 fixed in the well-resolved range at $G^2 = 0.1$. When $K^2 < G^2$, the spurious solution is mixed numerically with the exponentially decaying ($S^2 < 0$) physical solution. The possibility of a well-resolved ($S^2 < 0.4$) spurious mode (type A) can be seen for very small $K^2 > 0$, an imperfect emulation of set $S1$. In Fig. 2 the type B spurious modes (higher S^2) can also be seen to be supported at higher K^2, approaching spurious undamped short-wavelength wrinkles in the limit $K^2 = C_y^2G^2$. As G^2 decreases, these approach the limit G^2

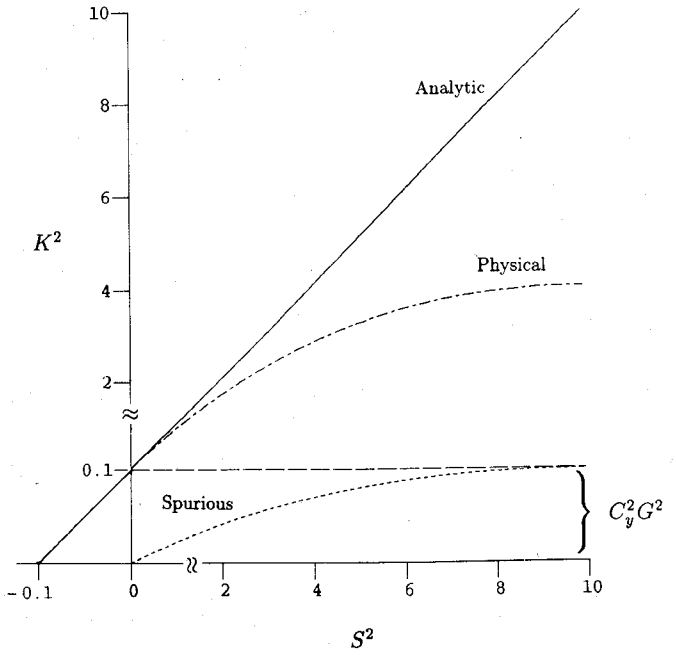

Fig. 2. K^2 versus S^2 for the FDD scheme with a fixed (well-resolved) $G^2 = 0.1$. Note the scaling breaks in the K^2 and S^2 axes near the origin. The "spurious" curve shows nonzero K^2 values over the full range of $S^2 > 0$.

$= 0$, $S^2 = \pi$ at $K^2 = 0$ (i.e., a constant in the y direction and an undamped wave of length $2h$ in the x direction.

In Fig. 3 we display contours of K^2 in (S^2, G^2) space. In the well-resolved zone A, the physical root gives qualitative fidelity to the analytic solution; and type A spurious solutions are supported for very low $K^2 < 0.04$. We use this limit to define "small" K^2. Type B spurious modes are evident at either end of the K^2 contours in zones B of the first quadrant, and are supported for $K^2 < 0.40$. We define this as the limit of "moderate" K^2. Type C spurious modes (poor resolution in both directions) are supported at "large" K^2, above 0.4. Since these large values would be avoided in most reasonable computations, these modes are of less interest than those of types A and B. Note that over the full range of quadrant I both the physical and spurious roots saturate at $K^2 = 4.0$.

For driven problems, K^2 is fixed and the dispersion relation is the composite of two constant K^2 contours—one physical and one spurious. We illustrate such composites in Fig. 4 for small and moderate values of K^2. Problems with large contrast in dielectric constant at material interfaces will have two values of K^2 present at an interface, with continuity conditions requiring the matching of the Fourier spectrum across the interface. Comparison of parts (a) and (b) of Fig. 4 suggests that in such a situation extremely spurious behavior on the low K^2 side could coexist with largely physical behavior on the high K^2 side. This is borne out in computational experiments [7].

The two roots K^2 in (36) support different (E_x, E_y) modes, or equivalently, (D, C) modes. Since the latter are of more direct interest, we reexpress (34) in terms of (D, C) using the definitions (6) and (7):

$$\begin{bmatrix} C_y^2G^2 - K^2 & -B_yB_xGS \\ -B_xB_ySG & C_x^2S^2 - K^2 \end{bmatrix} \begin{bmatrix} S & -G \\ G & S \end{bmatrix} \begin{Bmatrix} D \\ C \end{Bmatrix} = \begin{Bmatrix} 0 \\ 0 \end{Bmatrix}. \quad (39)$$

Substitution of K^2 from (36) allows solution of (39) for the ratio C/D as a function of (S, G) for the physical and spurious modes in turn. A plot of C/D for the spurious modes appears in Fig. 5. These modes are clearly *close* to $C = 0$ everywhere, with C/D peaking at 0.01 in zone A and at 0.2 in zone B. Both type A and B spurious modes may therefore be characterized approximately as divergence modes. It is easy to show from (39) that D/C for the physical modes is identical to $-C/D$ for the spurious modes, confirming that the physical modes are *nearly* divergence-free. This classification is not pure, however, and specification of physical boundary conditions with, for example, $D = 0$ will *necessarily* invoke a blend of physical and spurious modes. In effect, specification of physical boundary conditions guarantees the presence of unphysical features on the interior.

Finally, the increasing influence of parasites at low K^2 is of fundamental importance. The threshold of engineering accuracy is at $K^2 \equiv (kh)^2 = 0.4$, i.e., about ten nodes per wavelength. This is also the threshold for type B parasites. The path to convergence then follows increasingly smaller values of K^2, necessarily encountering type A as well as type B parasites along the way.

B. FED Scheme

The FE version of (36) is qualitatively the same as the FD version, and appears in Fig. 6. The same basic corrupted structure is evident. Type A parasites occur for roughly $K^2 < 0.015$, and type B parasites for $K^2 < 0.40$. As in the FDD scheme, the presence of parasites is enhanced as K^2 becomes arbitrarily small.

V. Helmholtz Schemes

The difference equations for the Helmholtz schemes may be assembled by direct substitution from Table III into (16):

$$\begin{bmatrix} -A_yC_x^2\sigma^2 - A_xC_y^2\gamma^2 + A_xA_yk^2 & 0 \\ 0 & -A_yC_x^2\sigma^2 - A_xC_y^2\gamma^2 + A_xA_yk^2 \end{bmatrix} \begin{Bmatrix} E_{xij} \\ E_{yij} \end{Bmatrix} = \begin{Bmatrix} 0 \\ 0 \end{Bmatrix}. \quad (40)$$

This system admits only a single dispersion relation, with multiplicity 2:

$$k^2 = \kappa^2 = \frac{C_x^2}{A_x}\sigma^2 + \frac{C_y^2}{A_y}\gamma^2. \quad (41)$$

The quantity κ^2, identical to that introduced above at (37), is quite well behaved, increasing monotonically with S and G all the way to the Nyquist points. Plots of κ^2 appear in Fig. 7 (FDH) and Fig. 8 (FEH). Both are qualitatively correct in the well-resolved range; overall, their single-valued, monotonic behavior is free of the difficulties which permeate the FDD and FED schemes.

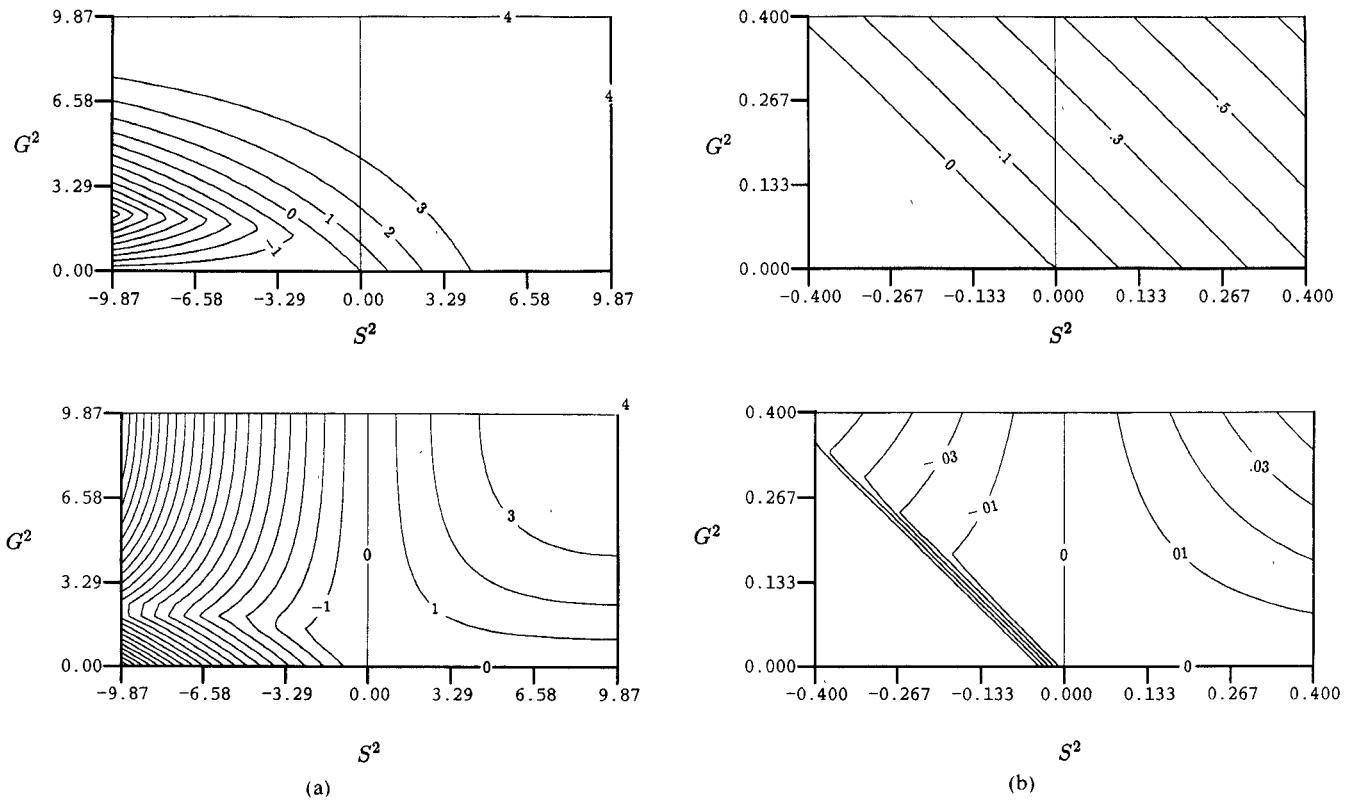

Fig. 3. (a) FDD contours of K^2 in (S^2, G^2) space. The full range: $-\pi^2 \leq S^2 \leq \pi^2$, $0 \leq G^2 \leq \pi^2$ is shown for the physical (top) and spurious (bottom) modes. (b) FDD contours as in Fig. 3(a) for the well-resolved zone: $|S^2, G^2| \leq 0.4$.

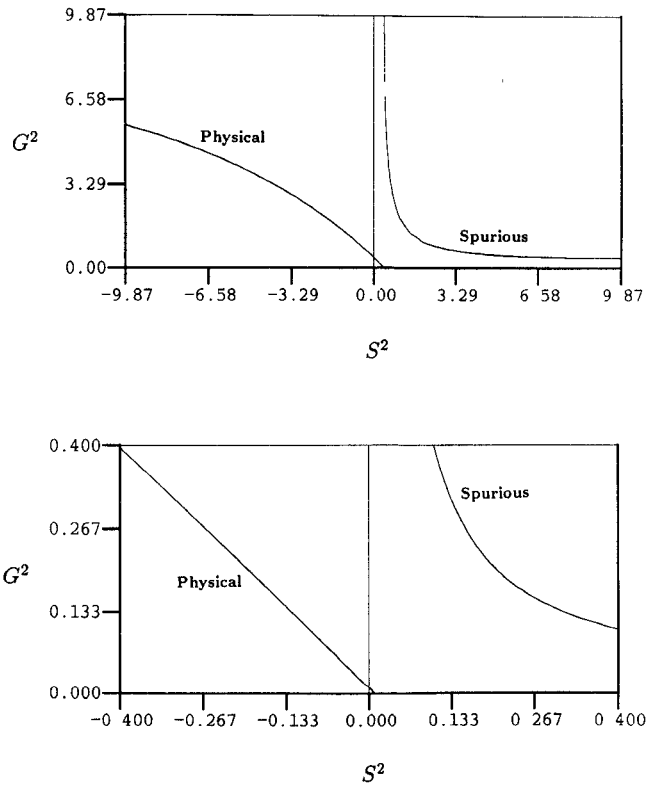

Fig. 4. Composite drawings of the physical and spurious FDD contours for a single value of K^2 illustrating its double-valued nature. A "moderate" value of $K^2 = 0.4$ (*top*) and a "small" value of $K^2 = 0.01$ (*bottom*) are shown.

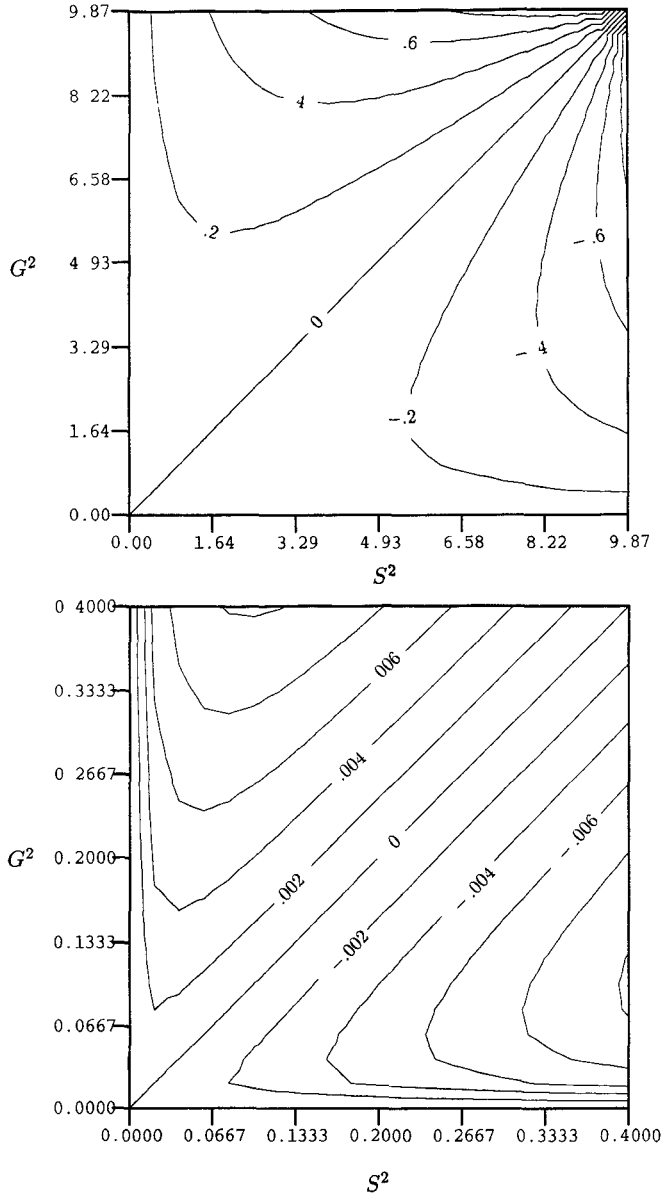

Fig. 5. Contours of C/D for the spurious modes, and equivalently, $-D/C$ for the physical modes, for the FDD and FDP ($p \neq 1$) schemes. Both the full range of quadrant I (*top*) and the well-resolved zone (*bottom*) are shown, illustrating the imperfect sorting of (D,C) modes for these schemes.

As in the analytic Helmholtz solutions, E_x and E_y are completely uncoupled, such that no interior constraints on D or C are enforced by the difference equations themselves. The physical and spurious modes may therefore be characterized as *pure curl* and *pure divergence* modes, respectively, perfectly emulating the analytic structure. As a result, specification of physical boundary conditions with $D = 0$ guarantees the absence of spurious modes.

VI. Penalty Schemes

Combination of the penalty method equation (20) with Table III yields the discrete form:

$$\begin{bmatrix} A_x C_y^2 \gamma^2 + pA_y C_x^2 \sigma^2 - A_x A_y k^2 & -(1-p) B_y B_x \gamma\sigma \\ -(1-p) B_x B_y \sigma\gamma & A_y C_x^2 \sigma^2 + pA_x C_y^2 \gamma^2 - A_x A_y k^2 \end{bmatrix} \begin{Bmatrix} E_{xij} \\ E_{yij} \end{Bmatrix} = \begin{Bmatrix} 0 \\ 0 \end{Bmatrix}. \quad (42)$$

Nontrivial solutions exist if

$$(k^2 - p\kappa^2)(k^2 - \kappa^2) + (1-p)^2 \epsilon^2 = 0 \quad (43)$$

where κ^2 and ϵ^2 are defined above at (37) and (38). As in the double-curl schemes, there are two roots:

$$k^2 = \left(\frac{1+p}{2}\right)\kappa^2 \pm \sqrt{\left(\left(\frac{1-p}{2}\right)\kappa^2\right)^2 - (1-p)^2\epsilon^2}. \quad (44)$$

As expected, this scheme reproduces the double-curl case for $p = 0$, and the Helmholtz case for $p = 1$. When p is "small," the behavior resembles that of the double-curl scheme, as demonstrated in Fig. 9, whereas when p is "large" both physical and spurious roots approach p times their respective values at $p = 0$, as seen in Fig. 10. In the latter case, the emulation of set $S2$ (eq. (24)) is grossly in error, shifted far from the correct values even in the well-resolved range.

D and C may be derived by substitution into (42) of (44) for k^2 and (6) and (7) for E_x and E_y. It is readily verified that, for $p \neq 1$, C/D is independent of p, and as discussed above for the FDD scheme, D/C for the physical modes is identical to $-C/D$ for the spurious modes. The scope of Fig. 5 is therefore significantly broadened. As a result, for all $p \neq 1$, the penalty scheme exhibits spurious modes with nonzero C and physical modes with nonzero D and necessarily invokes their blend in driven problems where $D = 0$ is physically correct. Only the unique value $p = 1$ collapses the two dispersion surfaces onto one, leaving D and C arbitrary, thereby allowing the perfect sorting of D and C modes described above for the Helmholtz equation.

VII. Primitive Maxwell Schemes

The discrete representation of the coupled primitive Maxwell equations, assembled directly from Table III and (27), are

$$\begin{bmatrix} i\omega\epsilon A_x A_y & 0 & iA_x B_y \gamma \\ 0 & i\omega\epsilon A_x A_y & -iA_y B_x \sigma \\ iA_x B_y \gamma & -iA_y B_x \sigma & i\omega\mu A_x A_y \end{bmatrix} \begin{Bmatrix} E_{xij} \\ E_{yij} \\ H_{zij} \end{Bmatrix} = \begin{Bmatrix} 0 \\ 0 \\ 0 \end{Bmatrix}. \quad (45)$$

For nontrivial solutions the requirement is

$$\omega\epsilon\left(k^2 - \left(\frac{B_x}{A_x}\right)^2 \sigma^2 - \left(\frac{B_y}{A_y}\right)^2 \gamma^2\right) = 0. \quad (46)$$

A. FDM Scheme

The emulation of $S1$ gives exactly $k^2 = 0$ here, unlike the shifted version obtained from the FDD scheme. This method is therefore free of type A vector parasites which originate uniquely in that feature. The emulation of $S2$ is intuitively appealing:

$$k^2 = B_x^2 \sigma^2 + B_y^2 \gamma^2. \quad (47)$$

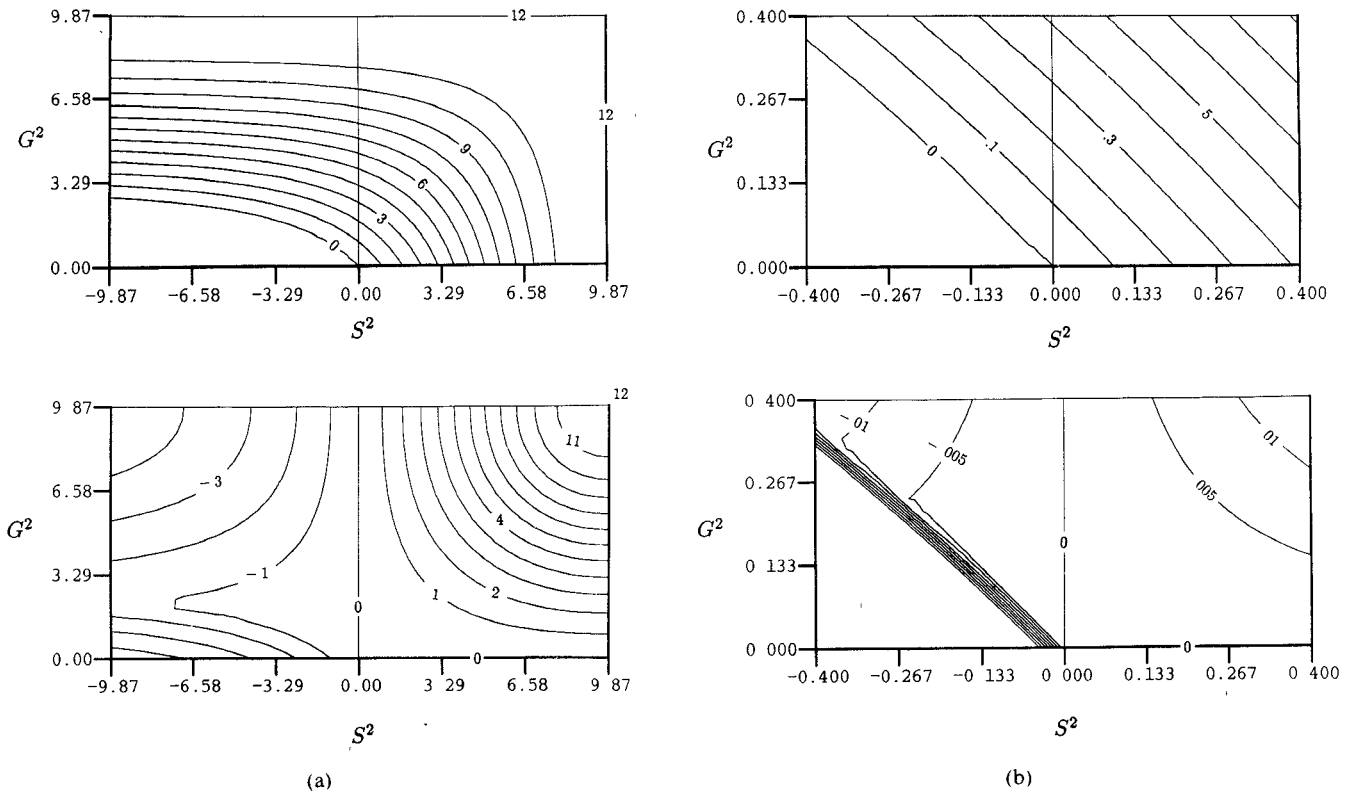

Fig. 6. (a) FED contours of K^2 in (S^2, G^2) space. The qualitative features are the same as that for the FDD discretization (see Fig. 3). Both the physical (top) and spurious (bottom) modes are shown over the full range $-\pi^2 \leqslant S^2 \leqslant \pi^2$, $0 \leqslant G^2 \leqslant \pi^2$. (b) FED contours as in Fig. 6(a) for the well-resolved zone $|S^2, G^2| \leqslant 0.4$.

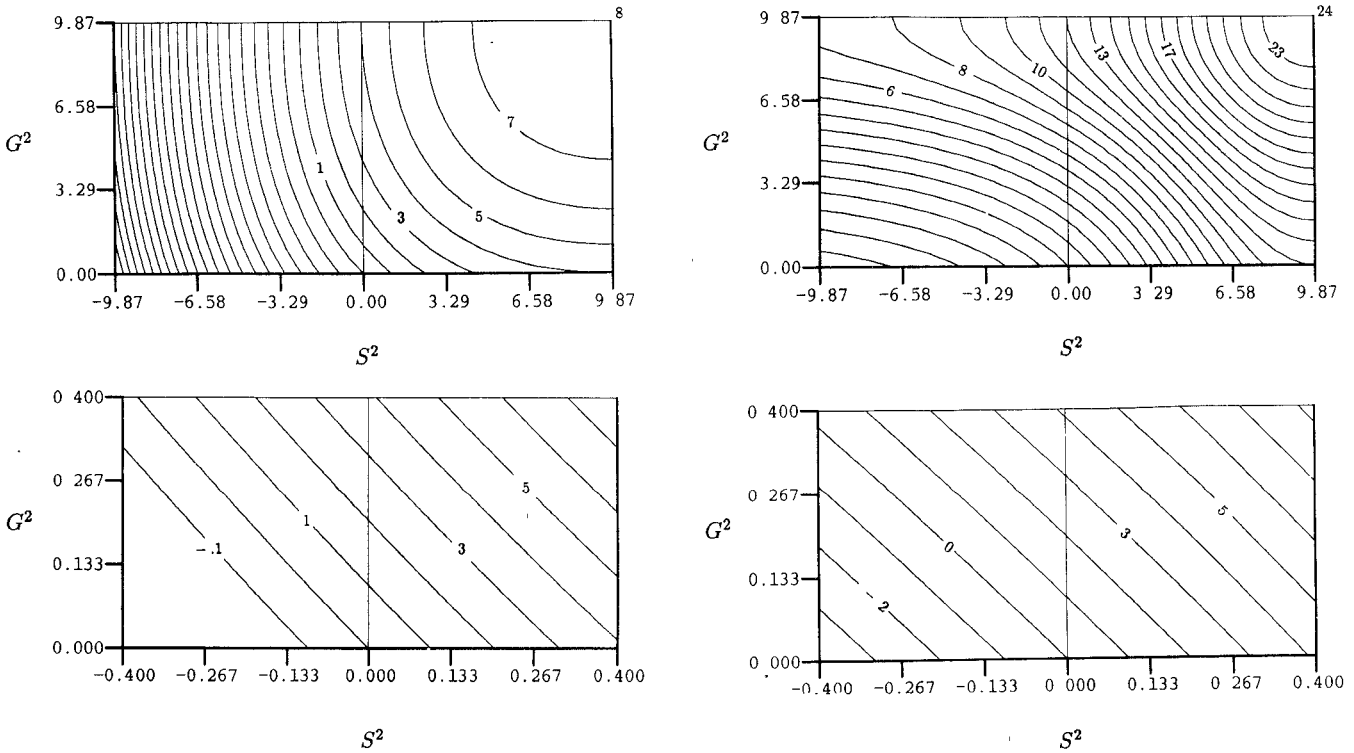

Fig. 7. FDH contours of K^2 in (S^2, G^2) space. The dispersion relation is monotonic over the full range (*top*) and mimics its analytic counterpart in the well-resolved zone (*bottom*). It is free of the difficulties illustrated in Figs. 3 and 4.

Fig. 8. FEH contours of K^2 in (S^2, G^2) space. Over the full range (*top*) the modes are monotonic and qualitatively correct in the well-resolved zone (*bottom*). This scheme is free of the difficulties illustrated in Fig. 6.

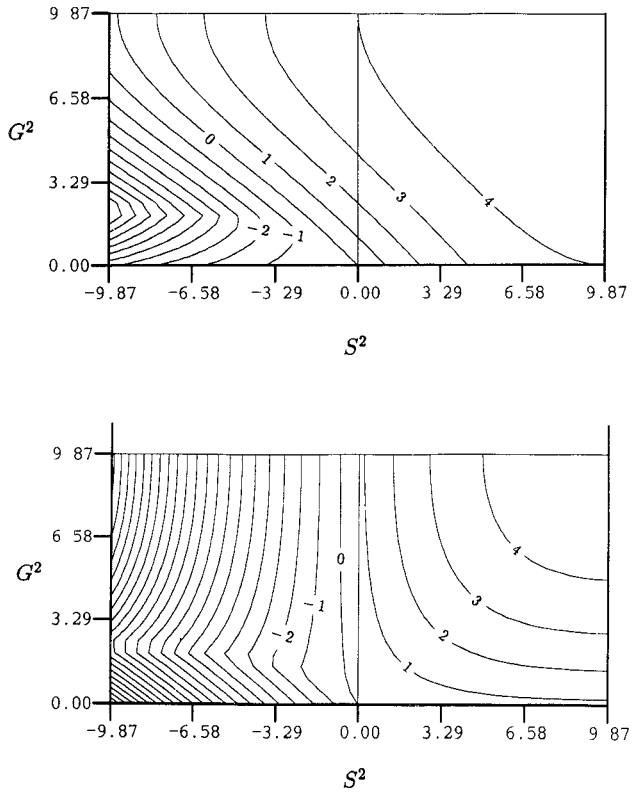

Fig. 9. FDP contours of K^2 with $p = 0.2$. Both the physical (*top*) and spurious (*bottom*) modes are shown

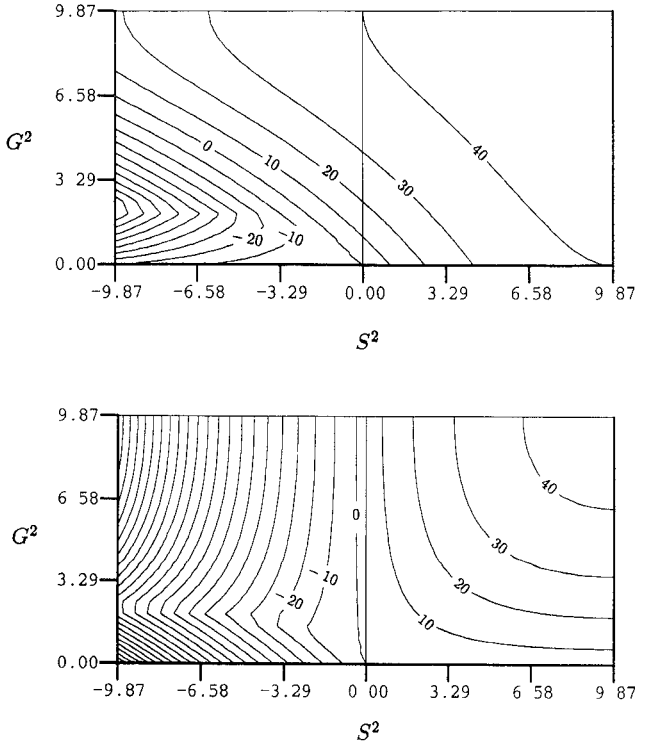

Fig. 10. FDP contours of K^2 with $p = 10$. Both the physical (*top*) and spurious (*bottom*) modes are shown.

At low (S, G), K^2 is monotonic and well behaved. However the folding of the B discretization factors at short wavelengths remains problematic. As can be seen in Fig. 11 this scheme is qualitatively faithful to the analytic for S and $G < \pi/2$, but like the FDD scheme there is confusion between short and long waves. The resulting contours of constant K^2 reveal type B parasites at $K^2 < 0.4$. These ought to be supported in the second or fourth quadrants, but the K^2 contours erroneously fold back into the first quadrant. Additionally, all small $K^2 > 0$ are supported in zone C (poorly resolved in both directions), a parasitic feature not found in the FDD scheme except at uninterestingly large K^2.

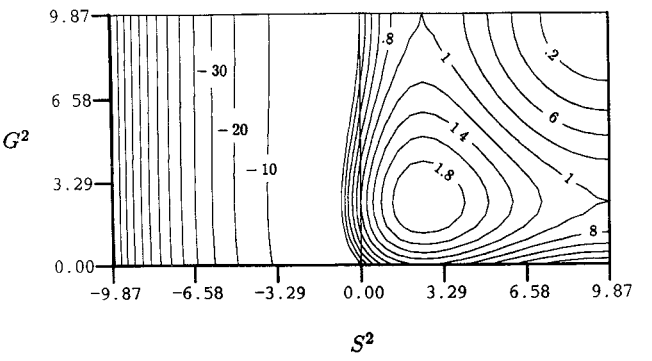

Fig. 11. FDM contours of K^2 in (S^2, G^2) space. For S and $G < \pi/2$, there is monotonic behavior which emulates the analytic dispersion relation; however, the folding of the B discretization factors gives rise to type B and C parasites when S or $G > \pi/2$.

This scheme is *potentially* fatally flawed. However, in its common implementation it is discretized on a staggered grid [8], [9]. The effect of the staggering is to truncate the Fourier spectrum at the effective Nyquist points $S, G = \pi/2$, thereby eliminating *all* of the spurious modes! Stated differently, the effective mesh spacing is doubled by the staggering; on the effective mesh $h' = 2h$, the dispersion relation (47) is identical to that for the FDH scheme on mesh spacing h':

$$k^2 = C_x'^2\sigma^2 + C_y'^2\gamma^2 \tag{48}$$

where the discretization factor $C_x' \equiv \sin(\sigma h'/2)/(h'/2)$. The FDM and FDH schemes have identical, parasite-free dispersion relations if the former is implemented on a staggered grid with the same *effective* mesh spacing.

B. FEM Scheme

As in the FDM scheme, the emulation of $S1$ is unshifted from $k^2 = 0$; the dispersion relation is monotonically faithful at low (S, G); and the folding of the B factors creates type B and C parasites in the range S or $G > \pi/2$. K^2 contours for this scheme appear in Fig. 12. For present purposes they are not essentially different from their FD counterparts.

While the FDM scheme deals effectively with the parasite problem by using a staggered mesh, there is no obvious, unique equivalent approach within the conventional FE framework. Indeed the FE method is often sought in an attempt to avoid the complications of the staggered grid, for example at boundaries or material interfaces. Unfortunately, a parasite-free dispersion relation cannot be obtained with simple, conventional FE discretization of the primitive equations, no matter how appealing that approach may be from other considerations. The construction of the FE equivalent of the staggered FD mesh remains an interesting and important area of research (e.g. [10] and [11]).

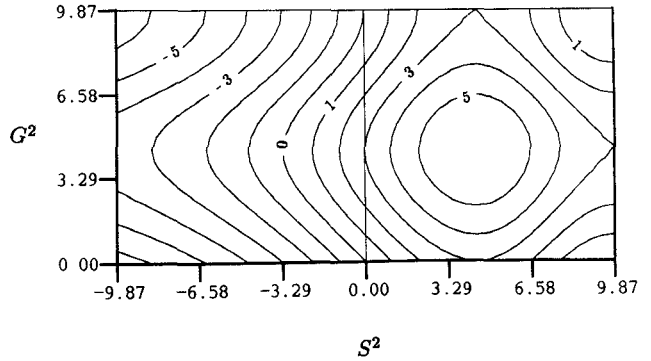

Fig. 12. FEM contours of K^2 in (S^2, G^2) space. Note the presence of type B and type C parasites for S^2 or $G^2 > (\pi/2)^2$ as in the FDM case (Fig. 11).

VIII. Discussion

The conventional 2-D finite difference and finite element methods examined here employ essentially similar discretization techniques. As a result they share the same structural behavior relative to vector parasites. In every case studied, parasites arise in the weakness of "leapfrogged" numerical derivatives—either the first derivative or the cross derivative. The main conclusions therefore concern the underlying form of the differential equations selected prior to discretization with these methods.

The double-curl schemes support double-valued dispersion relations, leading in turn to vector parasites of both type A and type B. The parasites become more pronounced as $(kh)^2$ becomes small. The root cause, numerically, is the cross-derivative term. At high resolution, this term converges slightly more slowly than the other second derivatives, leading to type A parasites. The type B parasites arise in its folding at low resolution. The imperfect sorting of physical and spurious modes in terms of (D, C) guarantees a spurious mode presence if physical boundary conditions are enforced for low and moderate values of K^2.

The vector Helmholtz schemes have monotonic dispersion relations of multiplicity 2, supporting both physical and spurious modes. The sorting of these into curl and divergence modes is, however, perfect. Specification of $D = 0$ in boundary conditions therefore guarantees the absence of spurious modes.

The penalty method is ineffective in eliminating vector parasites except in the special case $p = 1$, which reduces to the Helmholtz equation. At low p, the parasitic structure resembles that of the double-curl schemes; high p produces completely wrong results. For all $p \neq 1$, the sorting of the (D, C) modes is imperfect and independent of p.

The primitive Maxwell schemes produce folded dispersion relations, supporting type B and C vector parasites. This problem is completely eliminated by use of a staggered FD grid, and the dispersion relation in that case becomes identical to that of the FDH scheme with the same effective mesh spacing. Successful use of the FE method with the primitive equations depends critically on the correction or elimination of the folded first derivative terms, which are the root cause of the parasitic behavior.

In the FD arena, the use of the primitive equations with staggered grids is well established in time-domain applications. Helmholtz-based operators remain relatively unexplored for vector problems. For problems where precise positioning of boundaries and satisfaction of normal interface conditions are important, the Helmholtz approach with a nonstaggered grid is a promising alternative.

In the FE arena, vector Helmholtz operators and their generalizations offer unusual promise. Among the schemes considered, and within the limits of this idealized analysis, they alone are free of vector parasites when implemented on conventional scalar elements with correct boundary conditions. The conventional bases allow satisfaction of electromagnetic jump conditions at precisely placed boundaries and interfaces, one of the motivations for selecting the FE approach in general. In a separate paper [7] we present a general inhomogeneous FE method which reduces to the Helmholtz equation on homogeneous subregions, and demonstrate the elimination of type A and B parasites which infected comparable double-curl solutions. This approach has been implemented in 3-D in the time domain [18] and in the frequency domain [19]. Additional options within the FE framework may also prove promising, including the use of vector basis functions, staggered meshes, and mixed-interpolation elements.

The posing of normal boundary conditions required by FD or FE Helmholtz solutions actually demands no extra information. When Neumann tangential BC's are given (i.e., $\nabla \times \boldsymbol{E}$ or equivalently tangential $\boldsymbol{H}$,) the normal component of $\boldsymbol{E}$ is known exactly, *a priori*. A Dirichlet condition on E_n is therefore available. When Dirichlet conditions on tangential $\boldsymbol{E}$ are given, the condition $\nabla \cdot \boldsymbol{E} = 0$ provides the Neumann condition on E_n, i.e., $\partial E_n / \partial n$. In all cases, the process of specifying BC's for the Helmholtz equation involves only physical reasoning; while successful use of the double-curl, penalty, or primitive schemes would in principle rely on removal of unpredictable, spurious behavior which depends fundamentally on mesh details.

Finally, we note that while considerable attention has been paid to date to the eigenvalue spectrum of FE methods, less attention has been given to the associated eigenvectors. Clearly, spurious modes which are orthogonal to physical forcing have no presence in forced solutions. Additional future research could profitably focus on the character of the eigenvectors as well as the eigenvalues.

Acknowledgment

The authors wish to thank C. W. Crowley for initially calling their attention to the vector parasite problem.

References

[1] Z. J. Cendes and P. P. Silvester, "Numerical solution of dielectric loaded waveguides: I—Finite element analysis," *IEEE Trans. Microwave Theory Tech.*, vol. MTT-18, pp. 1124–1131, 1970.

[2] D. G. Corr and J. B. Davies, "Computer analysis of the fundamental and higher order modes in single and coupled microstrip," *IEEE Trans. Microwave Theory Tech.*, vol. MTT-20, 669–678, 1972.

[3] J. B. Davies, F. A. Fernandez, and G. Y. Philippou, "Finite element analysis of all modes in cavities with circular symmetry," *IEEE Trans. Microwave Theory Tech.*, vol. MTT-30, pp. 1975–1980, 1982.

[4] M. Koshiba, K. Hayata, and M. Suzuki, "Finite element formulation in terms of the electric field vector for electromagnetic waveguide problems," *IEEE Trans. Microwave Theory Tech.*, vol. MTT-30, pp. 900–905, 1985.

[5] A. Konrad, "On the reduction of the number of spurious modes in the vectorial finite-element solution of three-dimensional cavities and waveguides," *IEEE Trans. Microwave Theory Tech.*, vol. MTT-34, pp. 224–227, 1986.
[6] A. R. Pinchuk, C. W. Crowley, and P. P. Silvester, "Spurious solutions to vector diffusion and wave field problems," *IEEE Trans. Magn.*, vol. 24, pp. 158–161, 1988.
[7] K. D. Paulsen and D. R. Lynch, "Elimination of vector parasites in finite element Maxwell solutions," pp. 395–404, this issue.
[8] K. S. Yee, "Numerical solution of initial boundary value problems in isotropic media," *IEEE Trans. Antennas Propagat.*, vol. AP-14, pp. 302–307, 1966.
[9] A. Taflove and M. E. Brodwin, "Numerical solution of steady-state electromagnetic scattering problems using the time-dependent Maxwell's equations," *IEEE Trans. Microwave Theory Tech.*, vol. MTT-23, pp. 623–630, 1975.
[10] A. C. Cangellaris, C. C. Lin, and K. K. Mei, "Point-matched time-domain finite element methods for electromagnetic radiation and scattering," *IEEE Trans Antennas Propagat.*, 1160–1173, 1987.
[11] N. K. Madsen and R. W. Ziolkowski, "Numerical solution of Maxwell's equations in the time-domain using irregular nonorthogonal grids," *Wave Motion*, vol. 10, pp. 583–596, 1988.
[12] M. L. Barton and Z. J. Cendes, "New vector finite elements for three-dimensional magnetic field computation," *J. Appl. Phys.*, vol. 61, pp. 3919–3921, 1987.
[13] C. W. Crowley, P. P. Silvester, and H. Hurwitz, "Covariant projection elements for 3D vector field problems," *IEEE Trans. Magn.*, vol. 24, pp. 397–400, 1988.
[14] A. F. Peterson, "Finite element solution of the vector wave equation using divergenceless basis functions," in *Proc. 1989 IEEE AP-S Int. Symp.*, vol. III, pp. 1624–1627.
[15] A. Konrad, "A method for rendering 3D finite element vector field solutions non-divergent," *IEEE Trans. Magn.*, vol. 25, pp. 2822–2824, 1989.
[16] B. M. A. Rahman and J. B. Davies, "Penalty function improvement of waveguide solution by finite elements," *IEEE Trans. Microwave Theory Tech.*, vol. MTT-32, pp. 922–928, 1984.
[17] M. A. Morgan, "Coupled potentials for electromagnetic fields in homogeneous media," in *Finite Element and Finite Difference Methods in Electromagnetic Scattering*, M. A. Morgan, Ed. New York: Elsevier, 1990, pp. 211–247.
[18] D.R. Lynch and K. D. Paulsen, "Time-domain integration of the Maxwell equations on finite elements," *IEEE Trans. Antennas Propagat.*, vol. 38, pp. 1933–1942, Dec. 1990.
[19] X. Yuan, D.R. Lynch, and K. D. Paulsen, "Importance of normal field continuity in inhomogeneous scattering calculations," *IEEE Trans. Microwave Theory Tech.*, to be published.

Daniel R. Lynch received the B.S. and M.S. degrees in mechanical engineering from the Massachusetts Institute of Technology, Cambridge, in 1972 and the M.S. and Ph.D. degrees in civil engineering from Princeton University, Princeton, NJ, in 1976 and 1978, respectively.

He has worked as a power engineer and biomedical engineer, and he is currently Professor at Dartmouth College's Thayer School of Engineering, where he has taught since 1978. His interests are in environmental engineering and numerical analysis.

Keith D. Paulsen (S'85–M'86) received the B.S. degree in biomedical engineering from Duke University, Durham, NC, in 1981, and the M.S. and Ph.D. degrees in engineering from Dartmouth College, Hanover, NH, in 1984 and 1986, respectively.

He is currently an Assistant Professor in the Thayer School of Engineering at Dartmouth College. His research interests include numerical electromagnetics with application to biomedical problems.